PERGAMON

International Journal of Multiphase Flow 28 (2002) 635–663

International Journal of Multiphase Flow

www.elsevier.com/locate/ijmulflow

Segregation of granular flow in the transverse plane of a rolling mode rotating drum

Y.L. Ding [a,c,*], R. Forster [b,c], J.P.K. Seville [a,c], D.J. Parker [b,c]

[a] School of Chemical Engineering, University of Birmingham, Edgbaston, Birmingham B15 2TT, UK
[b] School of Physics and Astronomy, University of Birmingham, Edgbaston, Birmingham B15 2TT, UK
[c] Positron Imaging Centre, University of Birmingham, Edgbaston, Birmingham B15 2TT, UK

Received 14 March 2001; received in revised form 26 October 2001

Abstract

This paper reports some observations on the behaviour of a segregated particle bed consisting of a mixture of small and large particles in the transverse plane of a rolling mode rotating drum. A non-invasive positron emission particle tracking (PEPT) technique was used to follow the trajectories of different sized particles. A two-dimensional mathematical model based on the Eulerian approach and the thin layer approximation was developed to simulate solids motion and concentration distribution of different sized particles. It is shown that the bed structure for a binary mixture is similar to that for mono-sized particles, i.e. two-region structure consisting of a relatively thin 'active' region and a 'passive' region near the drum wall where particles move as a rigid body. At low rotational speeds, the velocity difference between small and large particles of a binary system is negligible in both the active and passive regions. At relatively high rotational speeds, the velocity difference is small in the active region and negligible in the passive region. Radial occupancy data suggest that small particles tend to concentrate in the core region, whereas large particles tend to occupy the shell region, in good agreement with model predictions. Axial occupancy data reveal that the axial particle mobility increases with drum rotational speed, and the mutual diffusivity of small particles is higher than that of large particles. It is also shown that the turnover time ratio of small to large particles is almost independent of concentrations of small particles under the conditions of this work.

Keywords: Particle segregation; Solids motion; Rotating drum; Rolling mode; Bed turnover time; Mathematical modelling; PEPT

* Corresponding author. Present address: Department of Chemical Engineering, University of Leeds, Leeds LS2 9JT, UK. Tel.: +44-113-233-2747; fax: +44-113-233-2405.
E-mail address: y.ding@leeds.ac.uk (Y.L. Ding).

0301-9322/02/$ - see front matter
PII: S0301-9322(01)00081-7

1. Introduction

Rotating drums play an important role in processing granular materials in the chemical, metallurgical, food and pharmaceutical industries, in which they are used to perform mixing, drying, heating and chemical reactions. However, a mixture of granular materials with different physical properties such as size, density, shape, roughness and resilience, tends to segregate (Williams, 1976). Such a phenomenon may have a significant impact on heat and mass transfer, and chemical reactions, and hence the productivity and product quality. Although the concept of rotating drums is simple, solids motion in such devices is very complicated, and six modes have been observed (Henein et al., 1983). With increasing rotational speed, they are slipping, slumping, rolling, cascading, cataracting and centrifuging modes. Particle segregation is expected to occur in all of these modes. As the rolling mode is often employed in industrial operations, this work is focused on this mode.

A considerable amount of experimental work on particle segregation in partially filled rotating drums has been carried out in the last few decades. The main conclusions can be summarised as follows:

1. Segregation occurs in both the radial and axial directions. Axial segregation proceeds slowly (usually after several hundred or even ten thousand drum revolutions), while radial segregation takes place rapidly (often within several drum revolutions); see for example, Donald and Roseman (1962), Rogers and Clements (1971), Henein (1987), Pollard and Henein (1989), Wightman and Muzzio (1998).
2. In the transverse plane, fine, rough and dense particles are found by most workers to concentrate in the core region of the bed (Pollard and Henein, 1989; Rogers and Clements, 1971). However, Wightman and Muzzio (1998) observed a different phenomenon, namely, large particles concentrate in segregated cores. For axial segregation, alternate bands of coarse and fine particles have been observed (Donald and Roseman, 1962; Rogers and Clements, 1971; Aranson and Tsimring, 1999a,b).
3. Segregation in the transverse plane occurs mainly through percolation, random sieving and expulsion, and trajectory mechanisms (Nityanand et al., 1986; Savage and Lun, 1988; Boateng and Bar, 1996), while the mechanism for axial segregation is still unclear. Bridgwater et al. (1985) and Hill and Kakalios (1995) attributed the axial segregation to the difference in repose angles of different sized particles, namely, the so-called trajectory mechanism. This mechanism, however, seems unable to explain the reversible process of the axial segregation.
4. There are some controversies regarding the kinetics of radial segregation. The results of Rogers and Clements (1971) and Cantelaube et al. (1997) showed that the kinetics of segregation was first-order, while Nityanand et al. (1986) observed a zeroth-order kinetics. Little work has been found in the literature on the kinetics of the axial segregation (Das Gupta et al., 1991; Nakagawa, 1994).

In parallel with the experimental work, mathematical modelling has also been carried out aiming at understanding the kinetics and mechanisms of particle segregation. These studies can be classified into the following two categories. The first category is the application of the Eulerian method, which treats the granular material as a continuum. The models of this category can be

divided further into two subcategories, namely, the stochastic diffusion model for axial direction segregation (Fan and Shin, 1979; Kudrna and Rochowiecki, 1988; Kudrna et al., 1992), and the continuous model for radial segregation (Boateng and Bar, 1996; Levitan, 1998; Aranson and Tsimring, 1999a,b; Puri and Hayakawa, 1999). The second category is the application of the Lagrangian approach (e.g. discrete element method and cellular automata), see for example Walton and Braun (1993), Yamane (1997), Cleary et al. (1998) and Ktitarev and Wolf (1999). These models help with interpreting some experimental observations. However, quantitative agreement between the model predictions and experiments has been rare in the published work.

The objectives of this work were focused on understanding solids motion and particle concentration distribution of a segregated bed in the transverse plane of a rotating drum operated in a rolling mode, and the effect of segregation on the macroscopic behaviour of the particle bed. A two-dimensional mathematical model based upon the Eulerian approach and the thin layer approximation was developed to investigate radial segregation. The model considered a horizontally positioned drum loaded with a binary mixture of small and large particles with identical density. The drum is operated in batch and in a rolling mode. A non-invasive positron emission particle tracking (PEPT) technique was used to follow particle motion and to validate the model. As radial segregation occurs rapidly, followed by a very slow axial segregation, the results of the two-dimensional model are expected to be applicable to cases where axial segregation has not occurred to an appreciable extent.

In Section 2, formulation of the two-dimensional model is presented. Details of the experimental work are given in Section 3. The results of experiments and model predictions are presented and discussed in Section 4, whereas the main conclusions are summarised in Section 5.

2. Theoretical

2.1. Formulation of the segregation model

Consider a horizontally positioned drum with less than 50% volumetric fill of a binary mixture of small and large particles of identical density (Fig. 1). The drum is operated in batch. Assuming that (a) convection and diffusion in the axial direction (z) are negligible due to batchwise operation; (b) the binary mixture is an incompressible continuum and small and large particles can penetrate through each other; and (c) the bulk velocity distribution does not change with concentration of small particles, then a mass balance on the small particles gives (Fig. 1)

$$\frac{\partial C_\mathrm{f}}{\partial t} + u\frac{\partial C_\mathrm{f}}{\partial x} + v\frac{\partial C_\mathrm{f}}{\partial y} + \frac{\partial[u_\mathrm{p}C_\mathrm{f}(1-C_\mathrm{f})]}{\partial x} + \frac{\partial[v_\mathrm{p}C_\mathrm{f}(1-C_\mathrm{f})]}{\partial y} = \frac{\partial}{\partial x}\left(D_x\frac{\partial C_\mathrm{f}}{\partial x}\right) + \frac{\partial}{\partial y}\left(D_y\frac{\partial C_\mathrm{f}}{\partial y}\right), \tag{1}$$

where C_f is the concentration of small particles, u and v are respectively, x- and y-wise components of the bulk velocity, u_p and v_p are percolation velocities of small particles in x- and y-directions, respectively, and D_i is diffusivity of fines in ith direction due to random motion ($i = x, y$). The fourth and fifth terms in the left-hand side of Eq. (1) are due to percolation (Gibilaro and Rowe,

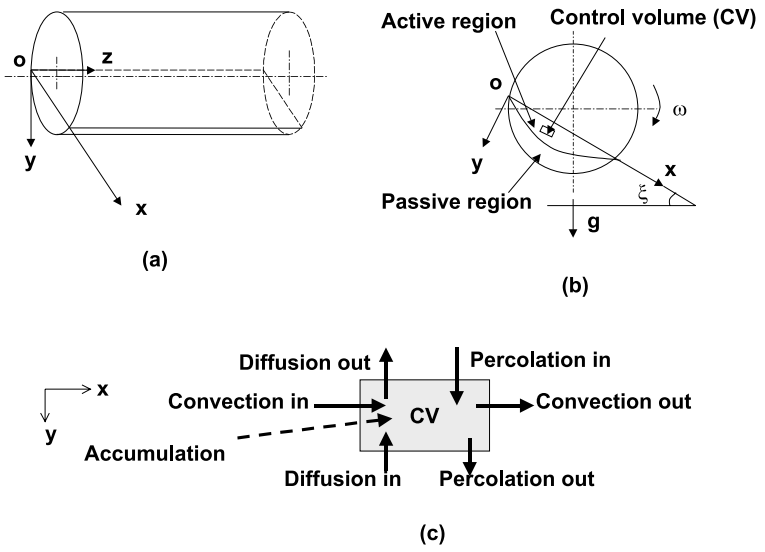

Fig. 1. Schematic diagram of a rotating drum and control volume for model formulation.

1974; Dolgunin and Ukolov, 1995; Boateng and Bar, 1996). The consequence of the assumptions leading to Eq. (1) will be taken up later on.

Eq. (1) is similar to but different from that obtained by Boateng and Bar (1996). In their derivation, the diffusivity and percolation velocity are assumed to be constant. As will be shown in the following, both the parameters are functions of shear rate (velocity gradient), the assumption made by Boateng and Bar (1996) is therefore only applicable to cases of linear velocity distribution. Solution to Eq. (1) requires (a) the bulk velocities u and v, (b) the percolation velocities u_p and v_p, and (c) the diffusivities D_x and D_y. These parameters will be discussed in the following sections.

2.1.1. Flow model for the bulk velocity

In theory, the bulk velocity can be obtained from the overall mass, momentum, and pseudo-energy equations:

$$\frac{\mathrm{d}\rho}{\mathrm{d}t} + \rho\nabla\cdot\vec{u} = 0, \tag{2}$$

$$\rho\frac{\mathrm{d}\vec{u}}{\mathrm{d}t} = \rho\vec{g} - \nabla\cdot\vec{p}, \tag{3}$$

$$\frac{3}{2}\rho\frac{\mathrm{d}T}{\mathrm{d}t} = -\vec{p}:\nabla\vec{u} - \nabla\cdot\vec{q} - \gamma, \tag{4}$$

where ρ is the bulk density of the granular material, $\vec{u}$ is the velocity vector, $\vec{p}$ is the pressure tensor, T is the granular temperature, $\vec{q}$ is the pseudo-energy flux due to conduction, γ is the energy dissipation due to inelastic particle collisions, and g is the acceleration due to gravity. However, solution to Eqs. (2)–(4) is often too complicated for design purposes as the available constitutive equations for $\vec{p}$, $\vec{q}$, and γ are very complicated in most practical cases and involve

many assumptions which are not always applicable to solids motion in rotating drums, see for example, Cowin (1974), Savage and Jeffrey (1981), Haff (1983), Jenkins and Savage (1983), Lun et al. (1984), Johnson and Jackson (1987), Savage and Hutter (1989), Anderson and Jackson (1992), Richman and Oyediran (1992), and Savage (1998). As a consequence, development of relatively simple models is required, which should be able to catch the main features of solids motion in rotating drums. For rotating drums filled with mono-sized particles and operated in a rolling mode, bed material can be divided into two regions in the transverse plane, namely, a thick 'passive' region near the drum wall and a relatively thin 'active' region in the upper part of the bed (Fig. 1(b)). In the passive region, particles move as a rigid body, and mixing and segregation are virtually negligible if the size ratio of small to large particles is larger than a critical value for the spontaneous percolation (0.1547, Bridgwater et al., 1985; Savage and Lun, 1988). As will be shown in Section 4, the two-region bed structure is also true for a binary mixture of small and large particles. As a consequence, the particle bed in the passive region can be described by the rigid body model. Solids mixing and segregation mainly occur in the active region where particles cascade down. As the active region is thin compared with the chord length, a thin layer approximation can be used to describe solids motion in this region, see for example, Khakhar et al. (1997), Elperin and Vikhansky (1998), Boateng (1998), and Ding et al. (2001a). Such an approximation has been shown to be able to provide a substantial simplification to the solution procedure without losing much accuracy (Boateng, 1998; Ding et al., 2001a). Due to different assumptions used by these workers, the resulting governing equations are different. The following integro-differential mass and momentum equations obtained by Ding et al. (2001a) for the steady-state batchwise operations is used in this work (see Appendix A for derivations):

$$\frac{\mathrm{d}}{\mathrm{d}x}\int_0^{\delta} u\,\mathrm{d}y = \omega\left[(L-x)-(h+\delta)\frac{\mathrm{d}\delta}{\mathrm{d}x}\right], \tag{5}$$

$$\frac{\mathrm{d}}{\mathrm{d}x}\int_0^{\delta} u^2\,\mathrm{d}y = \omega^2(h+\delta)\left[(h+\delta)\frac{\mathrm{d}\delta}{\mathrm{d}x}-(L-x)\right]+g\cos\xi(\tan\xi-\tan\beta)\delta, \tag{6}$$

where L is the half-chord length, h is the shortest distance between the drum centre and the bed surface, ω is the drum angular velocity, δ is the active layer depth, ξ is the dynamic repose angle (Figs. 1(b) and 2(a)), and β is the internal frictional angle. In the derivation of Eqs. (5) and (6), the following additional assumptions have been used: (a) bed surface is flat; (b) particles are non-cohesive; and (c) the centrifugal force is negligible compared with gravitational action. Note that Eqs. (5) and (6) only consist of the x-wise velocity, the y-direction velocity can be obtained from the differential continuity equation (Eq. (2)).

2.1.2. Percolation velocity model

As mentioned earlier, particle mixing and segregation mainly occur in the active region where particles cascade down the slope of the bed. This process bears some similarity to chute flows. As a consequence, the segregation model developed by Savage and Lun (1988) for inclined chute flows is adopted. This model considers the probability for forming a void in the underlying layer of a particle with a size large enough to capture the particle. It only gives the percolation velocity in the direction normal to the bed surface. In theory, percolation should occur in both x- and y-direction. However, the mass flux due to x-direction convection is expected to be much higher

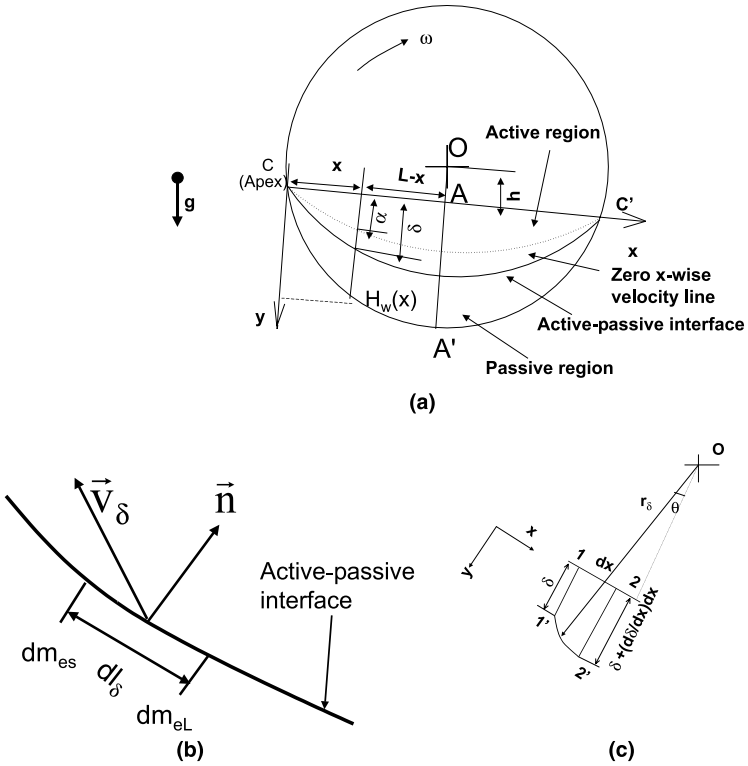

Fig. 2. Bed structure of a rotating drum operated in a rolling mode (a), the active–passive interface (b), and the control volume for flow model derivation (c).

than that due to percolation in this direction, u_p is therefore neglected. The net percolation velocity v_p determined by Savage and Lun (1988) has the following form:

$$v_p = v_{p0} d_{pl} \left(\frac{du}{dy} \right) \tag{7}$$

with v_{p0} given by

$$v_{p0} = \frac{4k_{LT}^2 \left(\frac{M}{N}\right)(1+\eta\sigma)}{\pi(1+\eta)(1+\eta\sigma^3)\left[\frac{(1+\eta)(1+\eta\sigma^2)}{(1+\eta\sigma)^2} + \left(\frac{\overline{E}^2}{k_{AV}}\right)\left(\frac{M}{N}\right)\right]} \cdot \Delta E, \tag{7a}$$

where

$$\Delta E = (E_b + \overline{E} - E_m + 1)\exp\left\{-\frac{E_b - E_m}{\overline{E} - E_m}\right\} - (E_a + \overline{E} - E_m + 1)\exp\left\{-\frac{E_a - E_m}{\overline{E} - E_m}\right\}. \tag{7b}$$

In Eqs. (7), (7a), and (7b), $\sigma = d_{ps}/d_{pl}$, d_{pl} and d_{ps} are sizes of the large and small particles, η is the number ratio of small to large particles, $E_a = (1+\eta)/(1+\eta\sigma)$, $E_b = (1+\eta)\sigma/(1+\eta\sigma)$, $\overline{E}$ is the mean void diameter ratio, k_{LT} is a layer-thickness constant close to unity, and M/N, E_m, and k_{AV} are constants depending on particle packing and have been given by Savage and Lun (1988). Eq.

(7) suggests that the percolation velocity is a function of the velocity gradient across the shear layer in the active region. As a consequence, v_p is normally not a constant except for linear velocity distribution.

2.1.3. Diffusion model

Due to shearing action, vigorous particle collisions may occur in the active region. The instantaneous velocity of a particle can be considered to consist of a mean velocity plus a fluctuation component. It is this fluctuation component that leads to the diffusive-like mass transfer. The summation of squares of fluctuation components in x-, y-, and z-direction also defines the granular temperature (see Eq. (4)). Theoretical work and experiments have shown that, in most part of the active region, the mean velocity in the x-direction is about an order of magnitude higher than that in the y-direction (see Section 4), and the shear rate $\mathrm{d}u/\mathrm{d}y$ is much higher than $\mathrm{d}v/\mathrm{d}x$ (Boateng, 1998). The diffusive action is therefore expected to be only significant in the y-direction, and D_x in Eq. (1) is ignored in this work. According to the kinetic theory, D_y can be given as

$$D_y = \frac{1}{2}\lambda \cdot v', \tag{8}$$

where v' is the fluctuation velocity in y-direction and λ is the mean free path of particles. The mean free path of particles can be approximated by the mean distance separating adjacent particles, s, which can be in turn linked to the solid volumetric fraction of the bed (Shen and Ackermann, 1982; Dolgunin and Ukolov, 1995):

$$\lambda \approx s = \left(\sqrt[3]{\frac{\pi}{3\nu_s}} - 1\right) d_{av}, \tag{8a}$$

where d_{av} is the average particle size defined as

$$d_{av} = d_{pl}(1+\eta\sigma)/(1+\eta) \tag{8b}$$

and ν_s is the solid volumetric fraction given as (Savage and Lun, 1988)

$$\nu_s = \frac{2(1+\eta)(1+\eta\sigma^3)}{3k_{LT}\left[1+\left(\frac{M}{N}\right)\left(\frac{\overline{E}^2}{k_{AV}}\right)\frac{(1+\eta\sigma)^2}{(1+\eta)(1+\eta\sigma^2)}\right](1+\eta\sigma^2)(1+\eta\sigma)}. \tag{8c}$$

Due to the thin nature of the active layer, the y-direction fluctuation velocity is approximated by the following expression developed by Shen and Ackermann (1982) for uniform rectilinear shear flows:

$$v' = l_p \frac{\mathrm{d}u}{\mathrm{d}y} \tag{8d}$$

with l_p given by

$$l_p = \left[\frac{(1+e_p)(0.05+0.08\mu_p)d_{av}^2(1+s/d_{av})}{\frac{3}{2}\frac{C_D\rho_f}{(d_{av}/s)\rho_p} + \frac{1}{8}(1-e_p^2) + \frac{1}{2\pi}\mu_p(1+e_p) - \frac{1}{8}\mu_p^2(1+e_p)^2}\right]^{1/2}, \tag{8e}$$

where C_D is the drag coefficient due to interstitial fluid, e_p is the restitution coefficient of particles, ρ_f is the density of interstitial fluid, ρ_p is the material density of particles, and μ_p is the kinetic friction coefficient. Eq. (8d) suggests that D_y is not a constant unless du/dy is constant (i.e. a linear velocity distribution).

2.2. Initial and boundary conditions for Eq. (1)

Eqs. (1), (2), (5)–(7), (7a), (7b), and (8) can be solved under appropriate initial and boundary conditions. As radial segregation usually occurs rapidly, i.e. a nearly steady state can be obtained in a short period of time, steady-state solution is considered here. Considering the cases without percolation and mixing in the passive region, the following boundary conditions suggested by Boateng and Bar (1996) can be used for concentration of small particles:

$$\text{At } y = 0 \text{ and } y = H_w(x) \text{ for } x \in (0, 2L), \quad C_f(x, y) = 0, \tag{9}$$

where $H_w(x)$ is the bed depth at x (Fig. 2(a)). Further discussion on the boundary conditions for the particle concentration will be given in Section 4. Solution of the flow model described in Section 2.1.1 also requires boundary or interface conditions, which are given in the following (Fig. 2(a)):

$$y = \delta, \ u = -\omega(h + \delta) \quad \text{(solid body motion at the active–passive interface)}, \tag{9a}$$

$$y = \alpha, \ u = 0 \quad \text{(corresponding to the flow reversal)}, \tag{9b}$$

$$y = 0, \ u = u_s \quad \text{(at the bed surface)}. \tag{9c}$$

2.3. Solution to the governing equations

Eq. (1) is applicable to both passive and active regions, while Eqs. (5)–(7), (7a), (7b), and (8) can only be used in the active region. In the passive region, $v_p = D_y = 0$.

2.3.1. Solution to the flow model

In brief, the procedure to solve Eqs. (2), (5), and (6) consists of the following four steps (more details are given in Appendix B, see also Boateng, 1998; Ding et al., 2001a):

- Step I: Select a suitable profile for u, usually, a polynomial or some other simple functions deduced from experiments. In this work, a second-order polynomial is adopted.
- Step II: Apply the boundary conditions, Eqs. (9a)–(9c) to the assumed form of the u profile to obtain the coefficients of the polynomial, which are functions of δ (active layer depth).
- Step III: Apply Eqs. (5) and (6) to obtain δ and therefore u.
- Step IV: Apply Eq. (2) to obtain v.

Depending on the rheological properties of bed material and shear rate, the flow in the active layer may mimic pseudo-plastic (indicated by slightly convex velocity profiles), Newtonian (linear velocity profiles), or dilatant (concave velocity profiles) behaviour. As dilatant flows are observed in most reported work on dry granular flows (Boateng and Bar, 1996; Ding et al., 2001a), only the concave velocity profiles are considered in this work. For dilatant flows, two cases may arise

depending on the value of $(\mathrm{d}u/\mathrm{d}y)|_{y=0}$. For drums loaded with spherical particles of relatively high restitution coefficients (e.g. glass beads) and operated at low to medium rotational speeds, bed dilation is small, $(\mathrm{d}u/\mathrm{d}y)|_{y=0}$ is approximately zero. In this case, the boundary condition Eq. (9c) can be replaced by $(\mathrm{d}u/\mathrm{d}y)|_{y=0} = 0$ and the velocity u can be written as (see Appendix B for derivation)

$$u = \frac{\omega(h+\delta)}{1-\Lambda^2}\left[\Lambda^2 - \left(\frac{y}{\delta}\right)^2\right], \tag{10}$$

where α is the zero x-wise velocity position (Fig. 2(a)), Λ ($\equiv \alpha/\delta$) is a parameter characterising the rheological behaviour of granular material, which lies within 0.75–0.90 at $x/(2L) = 0.10$ to 0.90 for a mono-sized particle bed (Boateng, 1998; Ding et al., 2001a). Substitution of Eq. (10) into Eq. (5), and considering $\delta = 0$ at $x = 0$, an analytical solution for δ can be obtained (see Appendix B for derivation):

$$\delta = \frac{1}{3\Lambda^2+1}\left[\sqrt{6(1-\Lambda^2)(3\Lambda^2+1)\left(Lx - \frac{x^2}{2}\right) + 4h^2} - 2h\right]. \tag{10a}$$

Note that the above analytical solution holds even if the parameter Λ is a function of x.

For drums operated at relatively high rotational speeds, a slightly curved bed surface may occur, and the surface cannot be regarded as a free surface if it is still assumed to be flat, i.e. $(\mathrm{d}u/\mathrm{d}y)|_{y=0} \neq 0$ (Johnson and Jackson, 1987; Boateng, 1998). In this case, Eq. (9c) has to be used and the following expression can be shown to give good approximation (see Section 4):

$$u = u_\mathrm{s} - \left[\frac{1+\Lambda}{\Lambda}u_\mathrm{s} - \frac{\Lambda}{1-\Lambda}\omega(h+\delta)\right]\left(\frac{y}{\delta}\right) + \left[\frac{u_\mathrm{s}}{\Lambda} - \frac{\omega(h+\delta)}{1-\Lambda}\right]\left(\frac{y}{\delta}\right)^2, \tag{10b}$$

where u_s is the surface velocity and is determined experimentally. The derivation of Eq. (10b) is given in Appendix B. Substitution of Eq. (10b) into Eq. (5) and application of the boundary condition $\delta = 0$ at $x = 0$ gives

$$\delta = \left\{ -\left[\frac{3\Lambda-1}{\Lambda}u_\mathrm{s} + \frac{4-3\Lambda}{1-\Lambda}\omega h\right] + \sqrt{\left[\frac{3\Lambda-1}{\Lambda}u_\mathrm{s} + \frac{4-3\Lambda}{1-\Lambda}\omega h\right]^2 + \frac{12\omega^2(2Lx-x^2)}{1-\Lambda}}\right\} \Big/ 2\left(\frac{\omega}{1-\Lambda}\right). \tag{10c}$$

Eqs. (10b) and (10c) can be simplified to give Eqs. (10) and (10a) if $(\mathrm{d}u/\mathrm{d}y)|_{y=0}$ is assumed to be zero. Note again that Eq. (10c) holds even if the parameter Λ and surface velocity u_s are functions of x.

2.3.2. Solution to the segregation model

Eq. (1) is a strong nonlinear partial differential equation and can be solved when the bulk velocity, percolation velocity and the diffusion coefficient are all determined a priori. The complete solution has to relay on the numerical method. By using an upwind scheme, Eq. (1) can be discretised to give the following finite difference equations (Fig. 3):

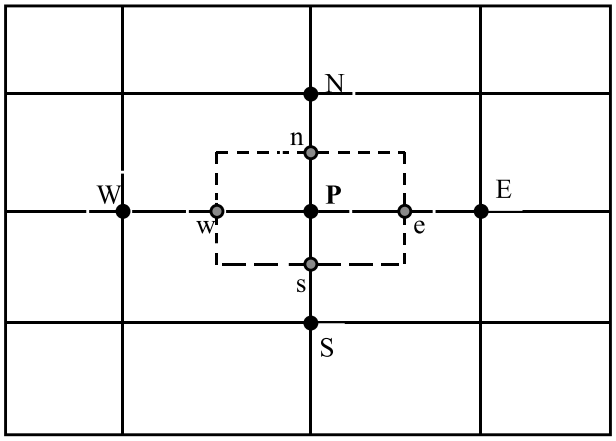

Fig. 3. Mesh of the spatial domain for numerical solution to Eq. (1).

$$A_P C_{fP} = A_E C_{fE} + A_W C_{fW} + A_S C_{fS} + A_N C_{fN} + b, \tag{11}$$

where A_i and b are given as

$$A_E = [|0.0, -u_E|]/\Delta x, \tag{11a}$$

$$A_W = [|0.0, u_W|]/\Delta x, \tag{11b}$$

$$A_N = [|0.0, v_N|]/\Delta y + D_{yn}/(\Delta y)^2, \tag{11c}$$

$$A_S = [|0.0, -v_S|]/\Delta y + D_{ys}/(\Delta y)^2, \tag{11d}$$

$$A_P = |u_p|/\Delta x + |v_p|/\Delta y + v_{PP} \cdot (1 - C_{fP})/\Delta y + D_{ys}/(\Delta y)^2 + D_{yn}/(\Delta y)^2, \tag{11e}$$

$$b_P = V_{PN}/\Delta y \cdot C_{fN} \cdot (1 - C_{fN}). \tag{11f}$$

In Eqs. (11a)–(11f) $[|i, j|]$ denotes the maximum of i and j, $|i|$ stands for absolute value of i, Δx and Δy are the mesh sizes in the x- and y-direction, and D_{yi} ($i = n$ and s) is the diffusivity at the interface of neighbour grids (Fig. 3) and can be obtained from the harmonic average of values at the main nodes.

2.3.3. Convergence criteria

The convergence criteria include: (a) the maximum difference in concentration of fine particles between two consecutive iterations is less than 10^{-6}; and (b) the total volume of fine particles in the whole bed is conserved within 0.1%.

3. Experiments

The experimental system used in this work consisted of a drum and associated driving and controlling unit (Fig. 4). The drum was placed horizontally between two γ-ray detectors of the newly equipped Birmingham positron camera. The detectors covered a field of $\sim 600 \times 600$ mm^2, and offered a spatial resolution of about 1mm and a time resolution of $<10^{-3}$ s under the con-

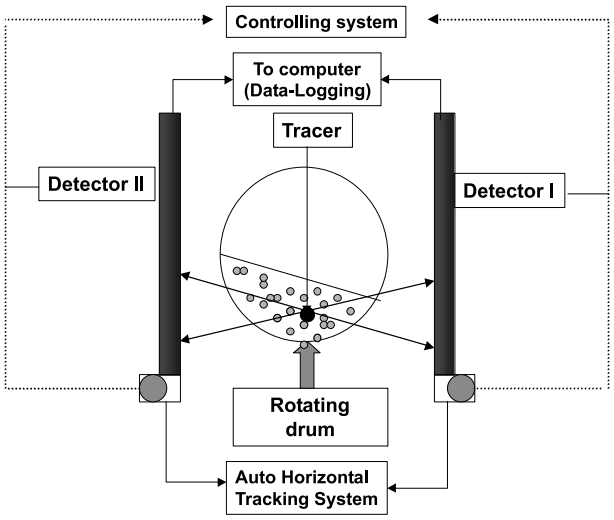

Fig. 4. Schematic diagram of the experimental system.

ditions of this study. A detailed description of the PEPT technique can be found elsewhere (Parker et al., 1993, 1997). But in brief, the PEPT technique makes use of a single radioactive tracer that carries positrons. Positrons annihilate with local electrons. This results in emission of back-to-back 511 keV γ-rays. Detection of the pairs of γ-rays enables the tracer location to be found by triangulation. The accuracy of the PEPT experiments in terms of measured velocities is mainly affected by particle velocity. For example, at a particle velocity of $\sim$1 m/s, the newly equipped camera at Birmingham offers an accuracy of $\sim$5%. As particle velocity is much less than 1 m/s in this work, the accuracy is expected to be better than 5%. As the PEPT technique only tracks one particle at a time, it is suitable for steady or very slow unsteady processes.

Drums with 240 and 400 mm inner diameters and 1000 mm length were used in this work. The cylindrical part of the drums was constructed with 'Perspex' acrylic glass. The inner walls of the cylinders were coated with a layer of sandpaper (grit 36) to prevent slippage between bed material and drum wall. The two end plates of the drum were made from aluminium, which were polished to minimise the end wall effect. The 240 mm drum was used for both solids motion and segregation studies, while the 400 mm drum was only used for solids motion studies.

Spherical glass beads with 1.5 ± 0.2 and 3.0 ± 0.2 mm diameter and a material density of ~ 2900 kg/m^3 were principally used in this work. For solids motion studies, 0.5 mm sand particles were also used in several runs. The tracers were made from particles taken from the bulk, and were activated by bombarding directly in the Birmingham in-house cyclotron: $^{16}\mathrm{O} + {}^{3}\mathrm{He} = {}^{18}\mathrm{F} + \text{neutron}$. ^{18}F decays by positron emission and has a half-life of $\sim$110 min. The particle tracking in each experiment lasted 1–2 h.

The PEPT measurements yield a large amount of data in terms of tracer's location as a function of tracking time, which after processing give instantaneous particle velocity and occupancy (defined as the ratio of the time that the tracer spends at a given position to the total tracking time). The concentration data are obtained by normalising the occupancy data of different sized tracers since a given position can only be occupied by either small or large particles at a given time. Due

to long tracking time, a tracer passes each point many times. The reported velocity and occupancy (concentration) data at a given point are therefore the average values at that point over the whole tracking time.

4. Results and discussion

4.1. Surface shape and dynamic repose angle for a binary mixture—PEPT measurements

Experimental work with a binary mixture of small and large particles has been carried out at drum volumetric fill of 14–26% and at rotational Froude number ($Fr = \omega^2 R/g$, R-drum radius) of $4.34 \times 10^{-4} - 1.2 \times 10^2$. Fig. 5 shows the typical map of velocity vectors in the transverse plane of the drum. A binary mixture of 20% 1.5 mm and 80% 3.0 mm glass beads was used in this run and the tracer was 3.0 mm in diameter. It can be seen that the bed surface is essentially flat except for the apex and the bottom end of the chord (C and C′ in Fig. 2(a)). From Fig. 5, the dynamic repose angle can be calculated to be 27°, which is ~1–2° higher than that for 1.5 mm glass beads (mono-sized) in a 400 mm diameter drum (Ding et al., 2001a). The dynamic repose angle was also found to be nearly independent of the rotational speed under the conditions of this study.

4.2. Velocity profiles and bed structure – PEPT measurements and model prediction

Fig. 6 shows the typical x-wise velocity profiles for a binary system of small and large particles across the bed depth at various x positions. It can be seen that the difference in x-wise velocities between the small and large particles is negligible at low drum rotational speed (Fig. 6(a)). At relatively high rotational speeds, the velocity difference is small in the surface layer (<15%) and negligible in the region near the drum wall (Fig. 6(b)). These results support the constant bulk

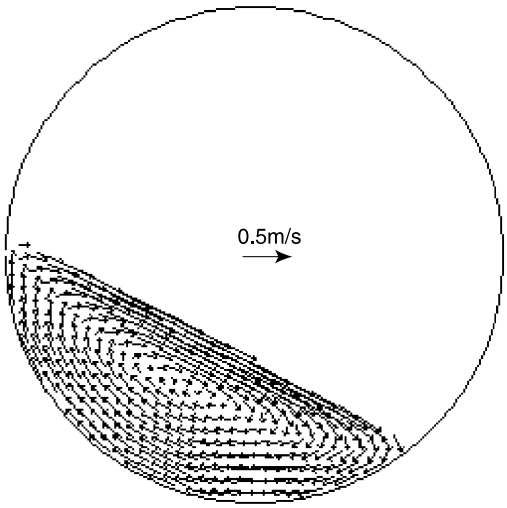

Fig. 5. Map of the velocity vectors for a binary mixture of 20% 1.5 mm and 80% 3.0 mm glass beads in a 240 mm drum operated at 9.6 rpm: 3.0 mm tracer, 26% fill by volume.

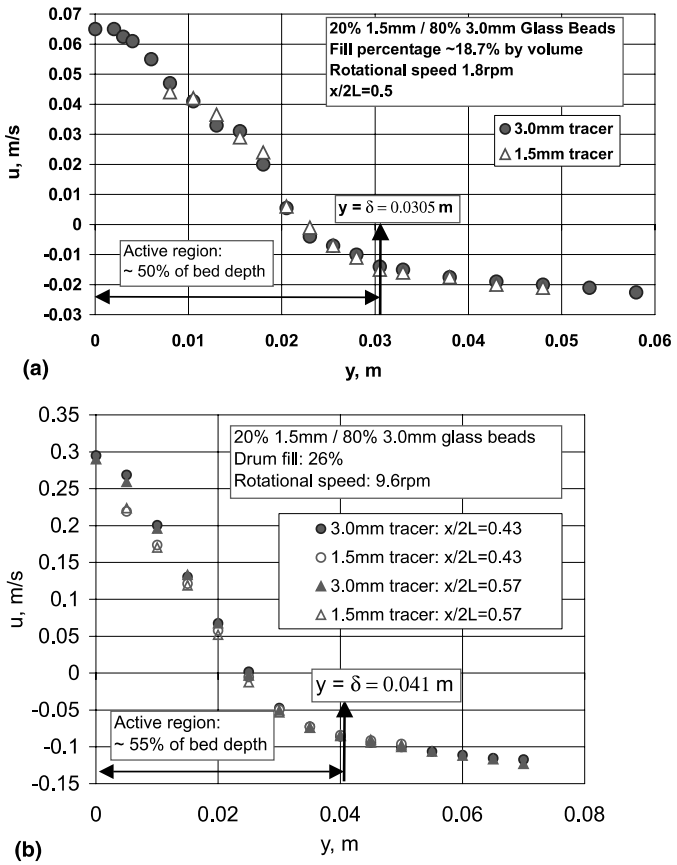

Fig. 6. Profiles of the x-wise velocity for small and large particles: PEPT measurements. (a) Low rotational speed, mid-chord position; (b) relatively high rotational speed, various x positions.

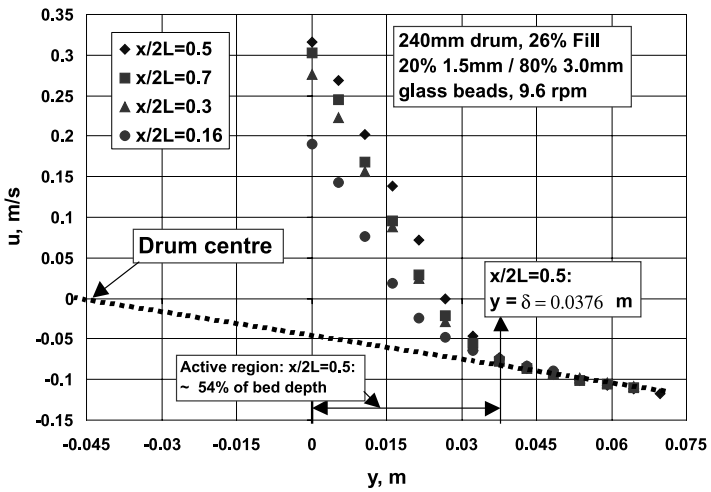

Fig. 7. X-wise velocity profiles of large particles at several x positions showing a two-region bed structure.

velocity assumption leading to the mathematical model described in Section 2. Fig. 6(a) also suggests that $(\mathrm{d}u/\mathrm{d}y)|_{y=0}$ approaches zero at low rotational speeds and Eq. (10) can be used to approximate x-wise velocity. This is in agreement with the results for mono-sized particles (Ding et al., 2001a). At the higher rotational speed (Fig. 6(b)), $(\mathrm{d}u/\mathrm{d}y)|_{y=0}$ is not zero. This indicates that Eq. (10b) has to be used to approximate the x-wise velocity profiles. The data points for small particles shown in Fig. 6 are limited to the core region of the particle bed, as little data were obtained in the outer shell region due to segregation. This lends support to the boundary conditions given by Eq. (9).

Fig. 7 shows the typical velocity profiles of large particles of a binary mixture at several x positions. It can be seen that a straight line from the drum centre goes through the data points near the drum wall. This indicates a two-region structure similar to that of a mono-sized particle bed, i.e. a 'passive' region near the drum wall where particles move as a rigid body, and an 'active' region. Fig. 7 also suggests that the active region is thin compared with the chord length of bed surface. The active region is not really 'thin' compared with the bed depth, which may account for

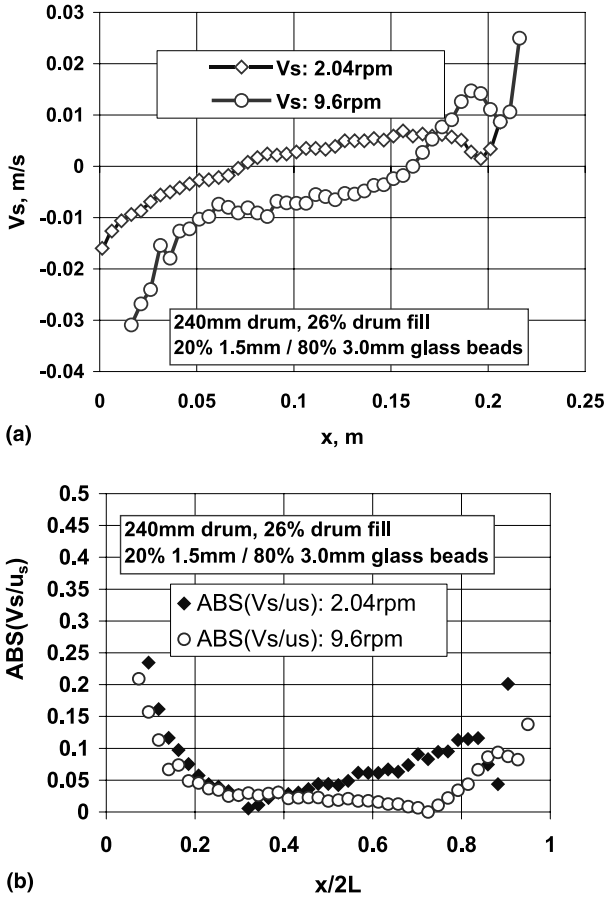

Fig. 8. Y-direction velocity of large particles at the bed surface and comparison with x-wise surface velocity. (a) Y-wise velocity at the bed surface; (b) comparison of x- and y-direction velocity at the bed surface.

over 50% of the bed depth, see Figs 6 and 7, where the active layer depth is indicated. It seems that the relative depth of the active region for binary system is larger than that for mono-sized systems, see Ding et al. (2001a) for data with mono-sized particles.

Fig. 8 shows the y-direction velocity profiles at the bed surface. In general, y-direction velocity is positive in the first half of the chord length and negative in the second half (Fig. 8(a)). Y-direction velocity is less than 15% of the x-wise velocity at $x/(2L) = 0.1$ to 0.9 (Fig. 8(b)).

It is interesting to compare the surface velocity of a rolling bed under different conditions. Fig. 9 shows the results for glass beads and sand. The results have been normalised in terms of the velocity at the mid-chord position ($x = L$). Two lines are parabolic functions of different powers – dashed line: $u_s/u_m = 1 - (1 - x/L)^2$, solid line: $u_s/u_m = [1 - (1 - x/L)]^2$. It can be seen that the shape of surface velocity profile for sand is different from that for glass beads, in particular in the 'first half' with the velocity profile for sand more flat. For glass beads, the surface velocity profile is symmetrical at low drum rotational speeds, but becomes more skewed towards to the 'second half' at higher rotational speeds. For sand particles, the 'first half' of the surface velocity profile cannot be represented by any of the two parabolic functions given above. This paper mainly deals with glass beads. Fig. 9 suggests that the dashed line fit the first half, whereas the solid line fit the second half of the experimental data points with glass beads reasonably well. Both the parabolic functions are therefore used in the flow model (Eq. (10b)). Such a treatment is expected to be more general.

Fig. 10 compares the predicted x-wise velocity and PEPT measurements at several x positions. In this figure, Eq. (10b) is used. It can be seen that good agreement has been achieved. Fig. 10 also suggests (indirectly) a good agreement between the model predictions and PEPT measurements of the active layer depth. At $x/2L = 0.5$, the measured active layer depth is 0.044 m for 240 mm drum

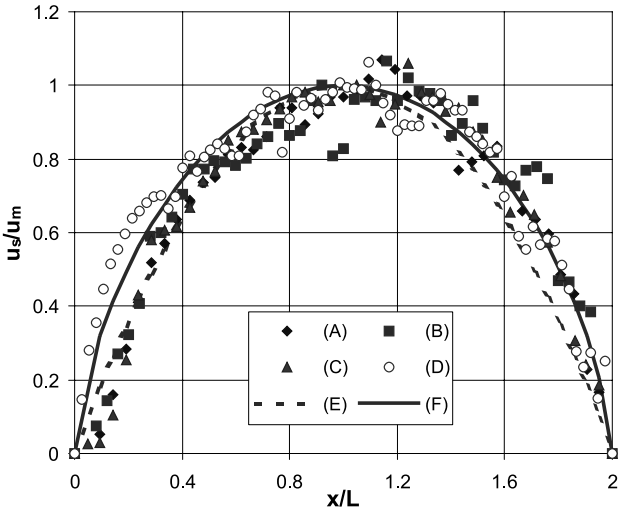

Fig. 9. Surface velocity profiles: (A) 240 mm drum, 26% fill of binary mixture of 20% 1.5 mm and 80% 3.0 mm glass beads, 9.6 rpm; (B) 400 mm drum, 7% fill of 1.5 mm glass beads, 0.8 rpm; (C) 240 mm drum, 14.7% fill of 3.0 mm glass beads, 7.5 rpm; (D) 400 mm drum, 30% fill of 0.5 ± 0.1 mm sand particles, 2 rpm; (E) Parabolic function $u_s/u_m = 1 - (1 - x/L)^2$; (F) Parabolic function $u_s/u_m = [1 - (1 - x/L)^2]^{2/3}$.

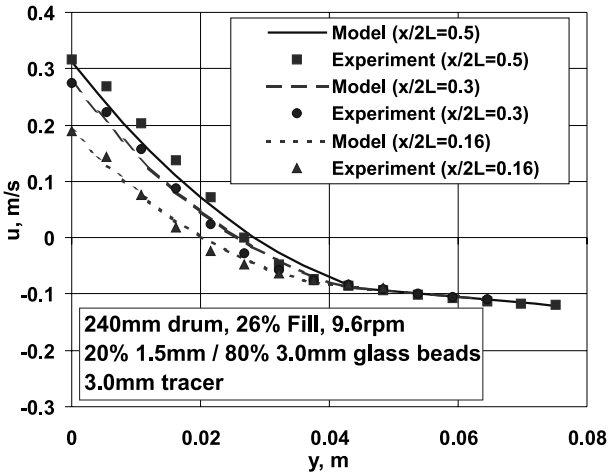

Fig. 10. Comparison between model predictions and PEPT measurements: x-wise velocity.

filled with 26% by volume of a binary mixture of 20% 1.5 mm/80% 3.0 mm glass beads and operated at 9.6 rpm, whereas the model predicted value is 0.0455 m. The difference is less than 3.5%.

4.3. Occupancy plot – PEPT measurements

As the PEPT technique involves the tracking of a single radioactive tracer, a parameter called occupancy has been proposed, which has been defined in Section 3. As mentioned in Section 3, the occupancy can be regarded as an indication of (and can be transformed to) the volumetric fraction of particles having the same size as the tracer.

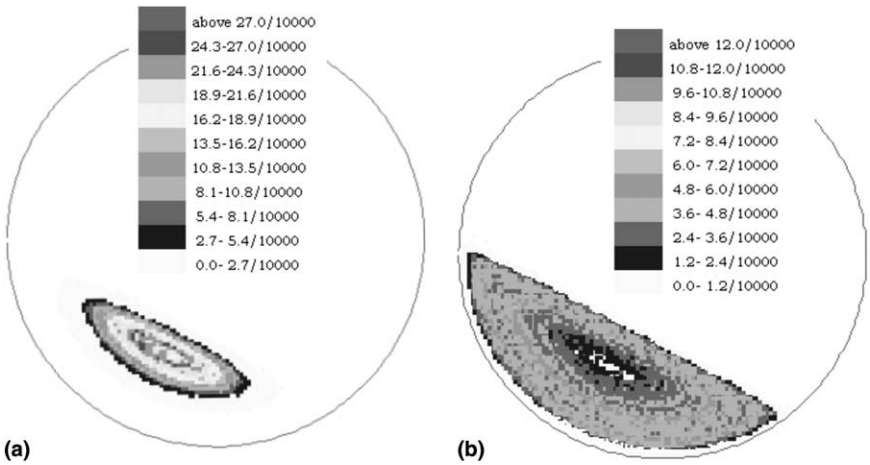

Fig. 11. Occupancy plots for (a) small and (b) large tracers in the transverse plane (20% 1.5 mm/80% 3.0 mm glass beads, 240 mm drum, 26% fill, 9.6 rpm, the numbers on the grey scale are occupancy data). (a) 1.5 mm tracer; (b) 3.0 mm tracer.

Typical occupancy plots of small and large tracers for a binary system in the transverse plane are shown in Fig. 11. A clear core-shell structure can be seen, which suggest small particles tend to occupy the core region of the bed (Fig. 11(a)), while large particles spend most of their time in the shell region (Fig. 11(b)). Fig. 11 also reveals a gradual change in the occupancies of both small and large tracers from the core to shell regions, an indication of diffusive-like mixing. The core-shell structure is bad for mixing operations but is not necessarily bad in terms of net effect in processes involving both heat transfer and chemical reactions. For example, in limestone calcination process, small particles react faster than larger ones at a given temperature. Due to segregation, small particles concentrate in the core region and they have little chance of reaching the bed surface where intensive heat transfer occurs. As a consequence, the temperature of small particles is lower than that of larger ones, which counteracts the fast reaction due to their smaller size. This suggests that a more uniform calcination of all particles could be achieved by using the segregation process.

Shown in Fig. 12 is the axial distribution of the occupancy for the small and large tracers. At the lower rotational speed (Fig. 12(c)), the tracer movement is restricted in a rather narrow range, indicating that the diffusion in the axial direction is very small. The range of tracer movement and

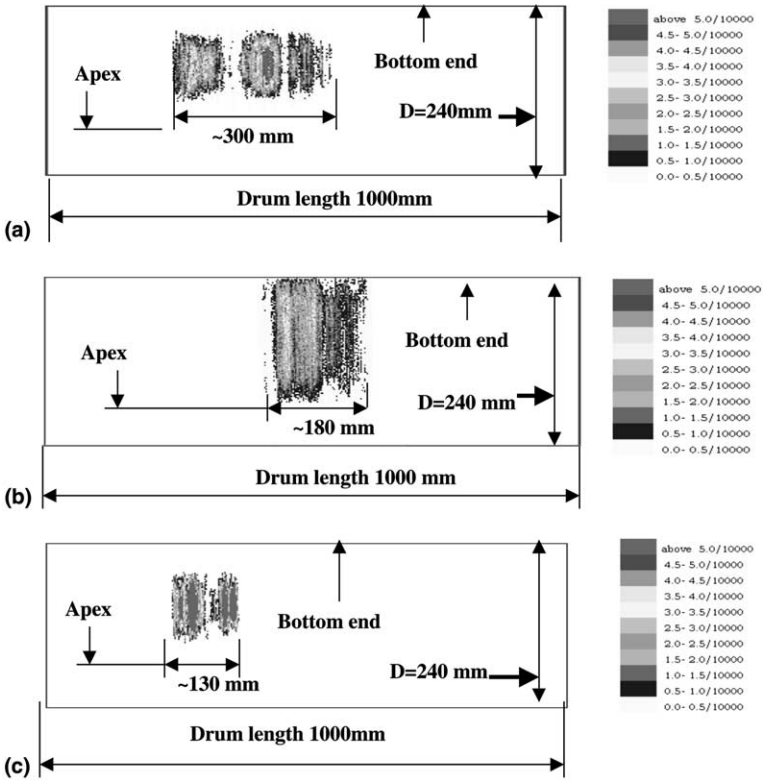

Fig. 12. Axial direction occupancy plots of small and large tracers: 20% 1.5 mm/80% 3.0 mm glass beads, 240 mm drum, 26% fill (the numbers on the grey scale are occupancy data). (a) 1.5 mm tracer, 9.6 rpm, tracking time = 4339 s; (b) 3.0 mm tracer, 9.6 rpm, tracking time = 4832 s; (c) 1.5 mm tracer, 1.8 rpm, tracking time = 4548 s.

hence the axial direction diffusion coefficient increases with rotational speed (Fig. 12(a)). If the axial direction movement of particles follows a random walk, then the diffusion coefficient (D_z) can be estimated by

$$D_z = \frac{1}{2}\sum \frac{(\Delta z)^2}{\Delta t}, \tag{12}$$

where $(\Delta z)^2$ is the mean square displacement of particles in the axial direction, Δt is the time interval. From the PEPT data, D_z is estimated at 10^{-5} m/s for 1.5 mm tracer at 9.6 rpm, 3.0×10^{-6} for 3.0 mm tracer at 9.6 rpm, and 1.8×10^{-6} m^2/s for 1.5 mm tracer at 1.8 rpm. The magnitude of these data is comparable with the results of mono-sized particles obtained by Koga et al. (1980), Hirosue (1980), and Parker et al. (1997) for rotation drums, and with Hwang and Hogg (1980) for chute flows. However, it is unclear if such a comparison is legitimate as binary mixtures are considered in this work. Moreover, the dependence of diffusion coefficient on particle size for binary systems is contrary to the results of Hirosue (1980) and Parker et al. (1997) who studied axial diffusion of mono-sized particles in rotating drums and found that the diffusion coefficient increased with particle size. Their results also appear to agree with the theoretical expression for particle self-diffusivity (D_s) in single-species granular flows (Hsiau and Hunt, 1996):

$$D_s = \frac{d_p\sqrt{\pi T}}{8(e_p+1)v_s g_0(v_s)}, \tag{12a}$$

where

$$g_0(v_s) = (1 - v_s/v_m)^{-2.5v_m} \tag{12b}$$

with v_m the maximum shearable solid volumetric fraction. The results obtained in this work are for binary system and are therefore the mutual diffusivities. Hsiau (2000) also derived an ex-

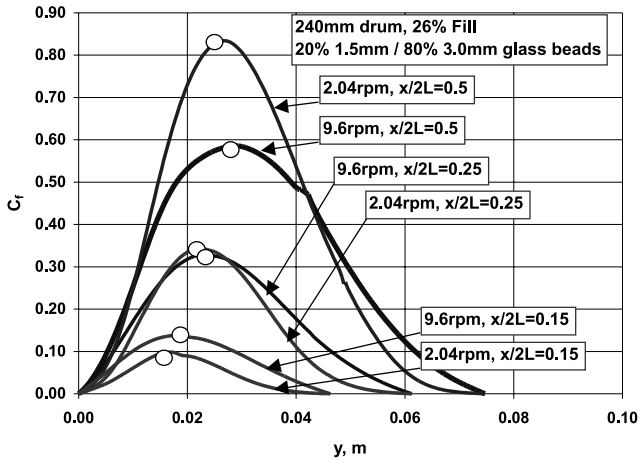

Fig. 13. Typical concentration distribution of small particles in the transverse plane: model prediction (for comparison purposes, measured positions of peak concentration of small particles are also included as circles).

pression for the mutual diffusivity, which is in inversely proportional to the square of the average particle diameter. More work is required in this aspect.

The non-uniform occupancy distribution in the axial direction is an indication of axial direction segregation. However, the highest occupancy of small tracers still occurs in the middle part of the bed, corresponding to the radial direction segregation. This suggests that axial direction segregation has not occurred to an appreciable extent under the conditions of these runs, possibly because the tracking time was less than 2 h and the total revolutions were less than 100–200, which may be not long enough to generate steady-state bands (Nakagawa, 1994).

4.4. Concentration distribution of small particles – model prediction and PEPT measurements

Fig. 13 shows the predicted y-direction concentration distributions of small particles in several x positions. The open circles in the figure represent the measured positions of the peak concentration of small particles. It can be seen that there exists a core region with high concentration of fine particles. The peak concentration is lower and the concentration distribution is more diffusive at high rotational speeds. This may be due to high diffusivity at high rotational speeds. The peak

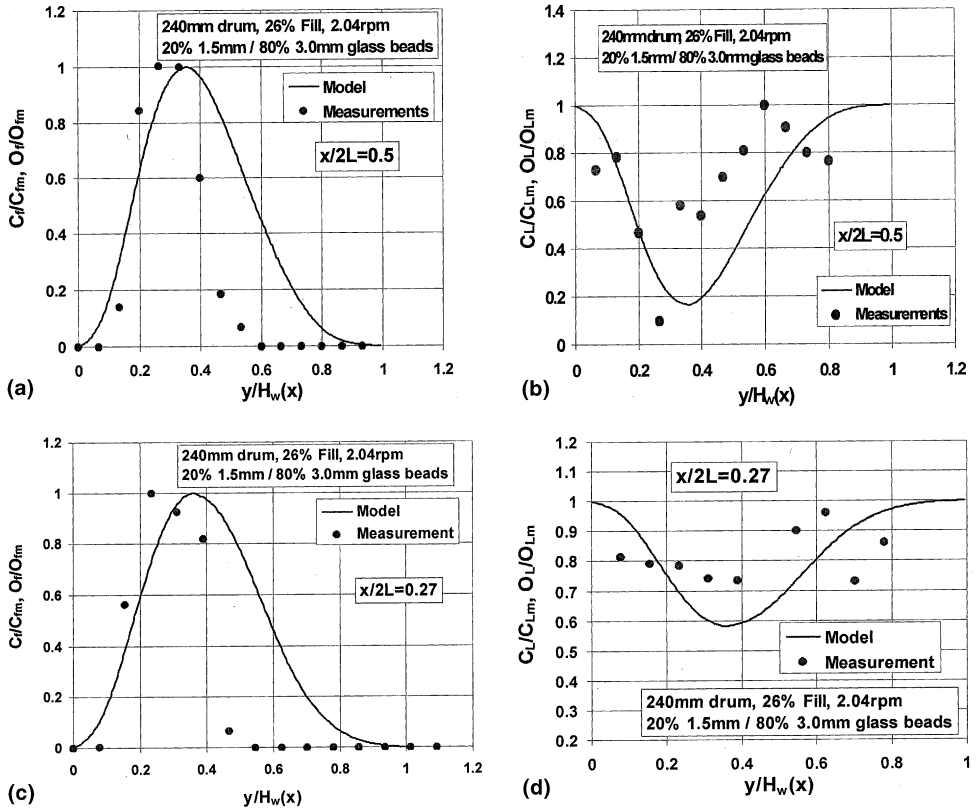

Fig. 14. Comparison between modelling and experiments – 2.04 rpm: (a) and (c) for small particles; (b) and (d) for large particles.

concentration occurs at $y/H_w(x) \sim 0.4$ when $x/(2L) \sim 0.1$ to 0.9, which agrees well with most experimental observations, see for example, Pollard and Henein (1989) and Rogers and Clements (1971). The small jerk in the right-hand side of the concentration peak is due to the active–passive interface where the diffusivity and percolation velocity are taken as zero.

Comparison between model predictions and PEPT measurements is shown in Figs. 13–15. In Figs. 14 and 15, C and O denote concentration and occupancy, respectively, subscripts f and L stand for small and large particles, and m denotes the maximum in a given x position. Reasonably good agreement can be seen for both the small and large particles in terms of the peak concentrations. However, there are considerable discrepancies in positions near the bed surface and drum wall, which can be attributed to several sources. Firstly, the diffusion model, Eq. (8), which contains two parameters, namely the mean free path of particles, and the fluctuation velocity. An expression developed by Shen and Ackermann (1982) for uniform rectilinear shear flows was used to calculate the fluctuation velocity. In the transverse plane of a rolling drum filled with a binary mixture, the size of the active layer accounts for a significant portion of the bed depth as shown in

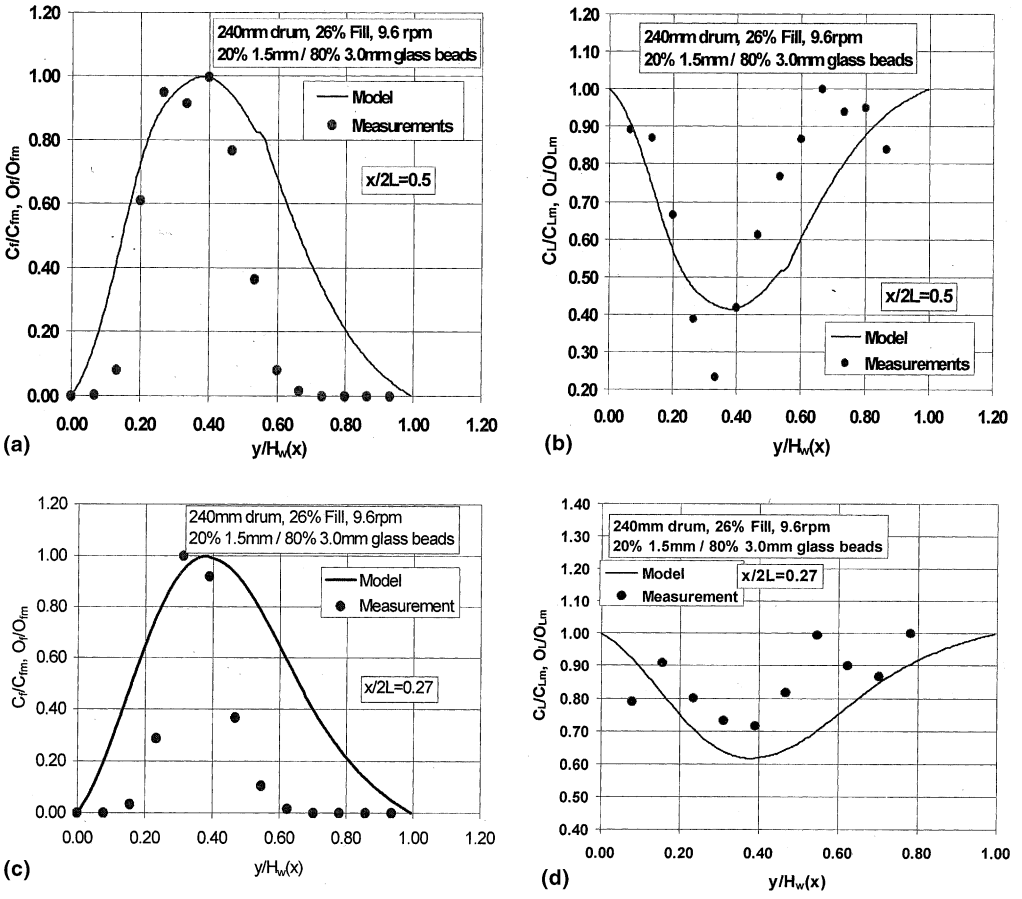

Fig. 15. Comparison between modelling and experiments – 9.6 rpm: (a) and (c) for small particles; (b) and (d) for large particles.

Figs. 6 and 7. This indicates that the flow in the cascading layer deviates considerably from uniformly rectilinear flow. Another possibility is that the formulation of the diffusion model itself. The diffusion model used in this work, Eq. (8), suggests that the diffusion is purely due to shearing action. According to Hwang and Hogg (1980), the diffusivity of shear granular flows is a linear function of shear rate which is not zero when the shear rate is zero. Secondly, the percolation model, Eq. (7), which was developed for chute flows. Although solids motion in rotating drums bears some similarity to chute flows, they are different, in particular in the 'second half' where particles decelerate.

4.5. Turnover time for small and large particles in a binary system

The turnover time is defined as the time required to turn the whole particle bed over once. It clearly has an important bearing on solids macroscopic mixing and heat transfer. A direct consequence of particle segregation is that the turnover time for small particles may differ from that of large particles. For mono-sized particles in both the slumping and rolling beds, bed turnover time has been derived by Ding et al. (2001b). For a binary system, the overall bed turnover time may also be determined in a similar way due to the weak dependence of the flow field on particle concentration. In the following, the turnover times for small and large particles are derived.

Consider a differential element $\mathrm{d}l_\delta$ of the active–passive interface as shown in Fig. 2(b), the net masses of small and large particles entering the active region through the interface per unit drum length per unit time are, respectively, given as

$$\mathrm{d}m_{\mathrm{eS}} = C_{\mathrm{f}\delta}\rho(\vec{v}_\delta \cdot \vec{n})\mathrm{d}l_\delta, \tag{13}$$

$$\mathrm{d}m_{\mathrm{eL}} = (1 - C_{\mathrm{f}\delta})\rho(\vec{v}_\delta \cdot \vec{n})\mathrm{d}l_\delta, \tag{13a}$$

where $\vec{v}_\delta$ is the velocity vector, $C_{\mathrm{f}\delta}$ is the concentration of small particles at the active–passive interface, and $\vec{n}$ is the unit vector normal to the active–passive interface. In writing Eqs. (13) and (13a), convection and diffusion in the axial direction of the drum and the radial direction diffusion at the passive–active interface are ignored. As particles move as a rigid body in the passive region, the x- and y-direction components of the velocity vector $\vec{v}_\delta$ can be given as (see Appendix A.1)

$$u_\delta = -\omega(h + \delta), \tag{13b}$$

$$v_\delta = -\omega(L - x). \tag{13c}$$

Combination of Eqs. (13), (13a)–(13c) gives

$$\mathrm{d}m_{\mathrm{eS}} = \omega\rho\left[(L - x) - (h + \delta)\left(\frac{\mathrm{d}\delta}{\mathrm{d}x}\right)\right]C_{\mathrm{f}\delta} \cdot \mathrm{d}x, \tag{14}$$

$$\mathrm{d}m_{\mathrm{eL}} = \omega\rho\left[(L - x) - (h + \delta)\left(\frac{\mathrm{d}\delta}{\mathrm{d}x}\right)\right](1 - C_{\mathrm{f}\delta}) \cdot \mathrm{d}x. \tag{14a}$$

Assume further that there is only one peak in $y = \delta(x)$ with the maximum depth, δ_{m}, occurring at $x = L$ (mid-chord), then integration of Eqs. (14) and (14a) gives, respectively, the total net masses of small and large particles entering the active region through the active–passive interface per drum length per unit time:

$$m_{eS} = \int_0^{m_{eS}} dm_{eS} = \int_0^L \omega\rho\left[(L-x) - (h+\delta)\left(\frac{d\delta}{dx}\right)\right] C_{f\delta} \cdot dx, \tag{15}$$

$$m_{eL} = \int_0^{m_{eL}} dm_{eL} = \int_0^L \omega\rho\left[(L-x) - (h+\delta)\left(\frac{d\delta}{dx}\right)\right] (1 - C_{f\delta}) \cdot dx. \tag{15a}$$

Experimental results have shown that $y = \delta(x)$ has only one peak at positions close to the mid-chord (Henein et al., 1983; Boateng and Bar, 1996; Ding et al., 2001a). Let M_L be the drum loading per unit length, which can be given as

$$M_L = \rho\left[R^2 \arcsin\left(\frac{L}{R}\right) - Lh\right]. \tag{16}$$

Then the total times required to turn over small and large particles once are given as

$$(t_{br})_S = \frac{M_L C_{f0}}{m_{eS}}, \tag{17}$$

$$(t_{br})_L = \frac{M_L (1 - C_{f0})}{m_{eL}}, \tag{17a}$$

where C_{f0} is the average concentration of small particles in the bed. Eqs. (15), (15a), (16), (17), and (17a) suggest that the bed turnover times of small and large particles are functions of drum rotational speed, drum fill level through L and h, the active layer depth and the concentration distribution. The active layer depth and the concentration distribution are unknowns and can be obtained from the model described in Section 2. For mono-sized materials, Eqs. (17) and (17a) reduce to the following form (analytical solution, Ding et al., 2001b):

$$t_{br} = 2[R^2 \arcsin(L/R) - Lh]/[\omega(L^2 - 2h\delta_m - \delta_m^2)]. \tag{18}$$

For the 240 mm drum filled with 26% by volume the binary mixture of 20% 1.5 mm and 80% 3.0 mm glass beads, application of Eqs. (17) and (17a) gives the turnover time of $(t_{br})_S = 2.65$ s, $(t_{br})_L = 3.05$ s at 9.6 rpm, and $(t_{br})_S = 11.9$ s, $(t_{br})_L = 14.0$ s at 2.04 rpm. It is also found that the turnover time ratio of small to large particles is nearly independent of the concentration of small particles. This seems to be a rather surprising result. In the following, an interpretation will be given.

Considering the mass fluxes of small and large particles in the active region through the mid-chord position (A–A′, Fig. 2(a)), one has

$$m_{eS} = \int_0^{\alpha_m} \rho C_f u \, dy, \tag{19}$$

$$m_{eL} = \int_0^{\alpha_m} \rho(1 - C_f) u \, dy, \tag{20}$$

where α_m is the zero x-wise velocity position at $x = L$. From Fig. 13, the concentration of small particles can be approximated by

$$C_f = (C_{fm}/y_m)y, \quad y \in [0, y_m], \tag{21}$$

where C_{fm} is the peak concentration of small particles at $(x, y) = (L, y_m)$, see Fig. 13. As y_m is approximately equal to α_m, substitution of Eqs. (10b) and (21) into Eqs. (19) and (20) gives

$$m_{eS} = \rho C_{fm} \Lambda_m \delta_m \left[\left(\frac{1}{6} - \frac{\Lambda_m}{12} \right) u_s + \frac{\Lambda_m^2}{12(1-\Lambda_m)} \omega (h + \delta_m) \right], \tag{19a}$$

$$m_{eL} = \rho C_{fm} \Lambda_m \delta_m \left\{ \left[\left(\frac{1}{2} - \frac{\Lambda_m}{6} \right) - \left(\frac{1}{6} - \frac{\Lambda_m}{12} \right) C_{fm} \right] u_s + \frac{\Lambda_m^2}{1-\Lambda_m} \omega (h + \delta_m) \left(\frac{1}{6} - \frac{C_{fm}}{12} \right) \right\}, \tag{20a}$$

where $\delta_m = \delta|_{x=L}$, and $\Lambda_m = \Lambda|_{x=L}$. Combination of Eqs. (17), (17a), (19a), and (20a) yields

$$\frac{(t_{br})_S}{(t_{br})_L} = \left\{ C_{f0} \left[2 + \frac{2u_s}{(2-\Lambda_m)u_s + \Lambda_m^2 \omega (h + \delta_m)/(1-\Lambda_m)} - C_{fm} \right] \right\} \Big/ C_{fm}(1 - C_{f0}). \tag{22}$$

As the term

$$\frac{2u_s}{(2-\Lambda_m)u_s + \Lambda_m^2 \omega (h + \delta_m)/(1-\Lambda_m)}$$

is not far from 1, Eq. (22) can be simplified further to give

$$\frac{(t_{br})_S}{(t_{br})_L} = \frac{C_{f0}(3 - C_{fm})}{C_{fm}(1 - C_{f0})}. \tag{22a}$$

Eq. (22a) provides an explanation to the very weak dependence of the bed turnover time on the concentration of small particles as the first and second terms in both the numerator and denominator compete with each other, e.g. an increase in C_{f0} leads to an increase in C_{fm}, but a decrease in both $(3 - C_{fm})$ and $(1 - C_{f0})$.

5. Conclusions

This paper is concerned with particle behaviour of a segregated bed in the transverse plane of a rolling rotating drum. A binary mixture of small and large particles with identical density is considered. The non-invasive PEPT technique is used to follow particle trajectories, from which the velocity and occupancy profiles can be obtained. A two-dimensional mathematical model based on the Eulerian approach and the thin layer approximation has been developed to simulate particle segregation. Theoretical expressions for the bed turnover time in terms of small and large particles are also derived. The following main conclusions are obtained:

- For a rolling drum loaded with a binary mixture of small and large particles, material bed can be divided into two regions, namely, a relatively thin active region on the upper part of the bed where particles cascade down, and a passive region near the drum wall where particles move as a rigid body. This is similar to a rolling bed consisting of mono-sized particles.
- At low rotational speeds, velocity difference between small and large particles of a binary mixture is negligible in both the active and passive regions. At relatively high rotational speeds, the velocity difference is small in the active region and negligible in the passive region.
- Surface velocity data in the direction parallel to the bed surface fit parabolic functions of different powers in the first half and second half of the chord of the bed surface.

- Surface velocity in the direction normal to the bed surface is less than 15% of that parallel to the bed surface in most part of the active region.
- Small particles have a high occupancy in the core region of the bed, while large particles tend to occupy the shell region.
- Axial mobility of particles increases with drum rotational speed. The mutual diffusivity of small particles is higher than that of large particles, which is different from the reported data for self-diffusion.
- The turnover time ratio of small to large particles is almost independent of concentrations of small particles.
- The model predictions agree reasonably well with experiments in terms of the peak concentration positions.
- Future work should be focused on the development of more general models for particle diffusion and percolation, and models for non-steady segregation process as well as experimental verification of these models.

Acknowledgements

Financial support form EPSRC (UK) under grant GR/M23083/01, Huntsman TiO_2 and United Biscuits is gratefully acknowledged. The authors also acknowledge the helpful comments of Professor J.F. Davidson and Dr. D.M. Scott of the University of Cambridge during biannual meetings on the EPSRC project on solids motion in rotating drums.

Appendix A. Derivation of the flow model

A.1. Integro-differential mass balance equation

With reference to Fig. 2(c), considering the control volume 1–2–2′–1′ and unit drum length, a mass balance gives

$$\boxed{\text{Mass flow out through } 2\text{–}2' = \text{Mass flow in through } 1\text{–}1',\ 1'\text{–}2',\ \text{and } 1\text{–}2} \tag{A.1}$$

Mass flow in through 1–1′:

$$\int_0^{\delta} \rho u \, \mathrm{d}y. \tag{A.1a}$$

Mass flow out through 2–2′:

$$\int_0^{\delta} \rho u \, \mathrm{d}y + \frac{\mathrm{d}}{\mathrm{d}x}\left(\int_0^{\delta} \rho u \, \mathrm{d}y \right) \mathrm{d}x. \tag{A.1b}$$

Mass flow in through 1′–2′:

$$\rho u_{\delta} \left(\frac{\mathrm{d}\delta}{\mathrm{d}x} \right) \mathrm{d}x - \rho v_{\delta} \mathrm{d}x. \tag{A.1c}$$

Mass flow in through 1–2 is zero (1–2 is bed surface). In Eqs. (A.1a)–(A.1c), u_δ and v_δ are the x-direction and y-direction velocities at $x = x$, $y = \delta$, respectively. At $x = x$, $y = \delta$, particles move as a rigid body with velocity ωr_δ, where r_δ is the radius. Decomposition of this velocity into x- and y-directions and considering the geometrical relations gives (Fig. 2(a) and (c))

$$u_\delta = -\omega r_\delta \cdot \cos\theta = -\omega(h + \delta), \tag{A.1d}$$

$$v_\delta = -\omega r_\delta \cdot \sin\theta = -\omega(L - x). \tag{A.1e}$$

Inserting Eqs. (A.1a)–(A.1e) into Eq. (A.1) and assuming constant bulk density, one has

$$\frac{\mathrm{d}}{\mathrm{d}x}\int_0^\delta u\,\mathrm{d}y = \omega(L - x) - \omega(h + \delta)\frac{\mathrm{d}\delta}{\mathrm{d}x},$$

which is Eq. (5) in the text.

A.2. Integro-differential momentum equation

Considering the same control volume (Fig. 2(c)), the momentum balance in the x-direction can be given as

$$\boxed{\text{Momentum flow out} - \text{Momentum flow in} = \text{Total force acting on the control volume}} \tag{A.2}$$

Momentum flow in through 1–1′:

$$\int_0^\delta \rho u^2\,\mathrm{d}y. \tag{A.2a}$$

Momentum flow out through 2–2′:

$$\int_0^\delta \rho u^2\,\mathrm{d}y + \frac{\mathrm{d}}{\mathrm{d}x}\left(\int_0^\delta \rho u^2\,\mathrm{d}y\right)\mathrm{d}x. \tag{A.2b}$$

Momentum flow in through 1′–2′ due to x-direction flow

$$\rho\omega^2(h + \delta)^2\left(\frac{\mathrm{d}\delta}{\mathrm{d}x}\right)\mathrm{d}x. \tag{A.2c}$$

Momentum flow out through 1′–2′ due to y-direction flow

$$\rho\omega^2(h + \delta)(L - x)\mathrm{d}x. \tag{A.2d}$$

The total force acting on the control volume in the x-direction

$$\rho g \sin\xi \cdot \mathrm{d}x\delta - P_{xy}|_{y=\delta}\,\mathrm{d}x, \tag{A.2e}$$

where P_{xy} is the shear stress acting on the surface 1′–2′ in x-direction. In writing Eq. (A.2e), the normal stress P_{xx} has been neglected. This is based on the dimensional analysis (Boateng, 1998).

For low and medium rotational speeds, the quasi-static contribution dominates so that the Coulomb frictional law is applicable, i.e. $P_{xy} = P_{yy}\tan\xi$. P_{yy} can be simply stated as $P_{yy} = [-\mathrm{sgn}(u)\cos\beta](\rho g)y$. Combination of these results and Eqs. (A.2a)–(A.2e) yields

$$\frac{\mathrm{d}}{\mathrm{d}x}\int_0^{\delta} u^2\,\mathrm{d}y = \omega^2(h+\delta)\left[(h+\delta)\frac{\mathrm{d}\delta}{\mathrm{d}x} - (L-x)\right] + g\cos\xi(\tan\xi - \tan\beta)\delta,$$

which is Eq. (6) in the text.

Appendix B. Derivations of Eqs. (10), (10a), (10b), and (10c)

Solution of the flow model consists of four steps, see Section 2.3.1 in the text. In the following, the details are given. Firstly, assuming that the x-direction velocity u has the following form (second-order polynomial):

$$u = a_0 + a_1 y + a_2 y^2, \tag{B.1}$$

where a_i ($i = 0$ to 2) are the coefficients. Then, inserting the boundary conditions given in the text, i.e. Eqs. (9a)–(9c), into Eq. (B.1):

$$-\omega(h+\delta) = a_0 + a_1\delta + a_2\delta^2, \tag{B.1a}$$

$$0 = a_0 + a_1\alpha + a_2\alpha^2, \tag{B.1b}$$

$$u_s = a_0. \tag{B.1c}$$

From Eqs. (B.1a)–(B.1c), the coefficient a_i ($i = 0$ to 2) can be obtained:

$$a_0 = u_s, \tag{B.1d}$$

$$a_1 = -\left[\frac{1+\Lambda}{\Lambda}u_s - \frac{\Lambda}{1-\Lambda}\omega(h+\delta)\right]\left(\frac{1}{\delta}\right), \tag{B.1e}$$

$$a_2 = \left[\frac{u_s}{\Lambda} - \frac{\omega(h+\delta)}{1-\Lambda}\right]\left(\frac{1}{\delta}\right)^2, \tag{B.1f}$$

where $\Lambda = \alpha/\delta$. Insertion of Eqs. (B.1d)–(B.1f) into Eq. (B.1) gives

$$u = u_s - \left[\frac{1+\Lambda}{\Lambda}u_s - \frac{\Lambda}{1-\Lambda}\omega(h+\delta)\right]\left(\frac{y}{\delta}\right) + \left[\frac{u_s}{\Lambda} - \frac{\omega(h+\delta)}{1-\Lambda}\right]\left(\frac{y}{\delta}\right)^2,$$

which is Eq. (10b) in the text. At low rotational speeds, $(\mathrm{d}u/\mathrm{d}y)|_{y=0} \to 0$. Application of this condition to Eq. (B.1) gives

$$0 = a_1. \tag{B.1g}$$

Combination of Eqs. (B.1a), (B.1b), and (B.1g) yields

$$a_0 = \frac{\omega(h+\delta)}{1-\Lambda^2}\Lambda^2, \tag{B.1h}$$

$$a_1 = 0, \tag{B.1i}$$

$$a_2 = -\frac{\omega(h+\delta)}{1-\Lambda^2}\left(\frac{1}{\delta}\right)^2. \tag{B.1j}$$

Insertion of Eqs. (B.1h)–(B.1j) into Eq. (B.1) gives

$$u = \frac{\omega(h+\delta)}{1-\Lambda^2}\left[\Lambda^2 - \left(\frac{y}{\delta}\right)^2\right],$$

which is Eq. (10) in the text. Inspection of Eqs. (10) and (10b) suggests that there are two unknowns, δ and Λ, which can be obtained theoretically from the mass and momentum integro-differential equations (5) and (6). Firstly, considering low drum rotational speeds, i.e. $(\mathrm{d}u/\mathrm{d}y)|_{y=0} = 0$, inserting Eq. (10) into Eqs. (5) and (6), one has

$$\frac{\mathrm{d}}{\mathrm{d}x}\left[\frac{3\Lambda^2-1}{3(1-\Lambda^2)}(h+\delta)\delta\right] = (L-x) - (h+\delta)\frac{\mathrm{d}\delta}{\mathrm{d}x}, \tag{B.1k}$$

$$\frac{\mathrm{d}}{\mathrm{d}x}\left[\frac{\Lambda^4 - \frac{2}{3}\Lambda^2 + \frac{1}{5}}{(1-\Lambda^2)^2}\delta(h+\delta)^2\right] = (h+\delta)^2\frac{\mathrm{d}\delta}{\mathrm{d}x} - (h+\delta)(L-x) + g\cos\xi(\tan\xi - \tan\beta)\delta/\omega^2. \tag{B.1l}$$

Solution to Eqs. (B.1k) and (B.1l) requires boundary conditions for both δ and Λ. The boundary condition for δ can be simply stated as $\delta = 0$ at $x = 0$. Under this constraint, Eq. (B.1k) is integrated to yield

$$\delta = \frac{1}{3\Lambda^2+1}\left[\sqrt{6(1-\Lambda^2)(3\Lambda^2+1)\left(Lx - \frac{x^2}{2}\right) + 4h^2} - 2h\right],$$

which is Eq. (10a) in the text. For $(\mathrm{d}u/\mathrm{d}y)|_{y=0} \neq 0$, a similar procedure to the above leads to Eq. (10c).

References

Anderson, K.G., Jackson, R.J., 1992. A comparison of the solutions of some proposed equations of motion of granular materials for fully developed flow down inclined planes. J. Fluid Mech. 241, 145–168.

Aranson, I.S., Tsimring, L.S., 1999a. Continuum theory of axial segregation in a long rotating drum. Phys. Rev. E 60, 1975–1987.

Aranson, I.S., Tsimring, L.S., 1999b. Dynamics of axial separation in long rotating drums. Phys. Rev. Lett. 82, 4643–4646.

Boateng, A.A., 1998. Boundary layer modeling of granular flow in the transverse plane of a partially filled rotating cylinder. Int. J. Multiphase flow 24, 499–521.

Boateng, A.A., Bar, P.V., 1996. Modelling of particle mixing and segregation in the transverse plane of a rotary kiln. Chem. Eng. Sci. 51, 4167–4181.

Bridgwater, J., Foo, W.S., Stephens, D.J., 1985. Particle mixing and segregation in failure zones—theory and experiment. Powder Technol. 41, 147–158.

Cantelaube, F., Bideau, D., Roux, S., 1997. Kinetics of segregation of granular media in a two-dimensional rotating drum. Powder Technol. 93, 1–11.

Cleary, P.W., Metcalfe, G., Liffman, K., 1998. How well do discrete element granular flow models capture the essentials of mixing processes? Appl. Math. Modelling 22, 995–1008.

Cowin, S.C., 1974. A theory for the flow of granular materials. Powder Technol. 9, 61–69.

Ding, Y.L., Forster, R.N., Seville, J.P.K., Parker, D.J., 2001a. Solids motion in the rolling mode rotating drums operated at low to medium rotational speeds. Chem. Eng. Sci. 56, 1769–1780.

Ding, Y.L., Forster, R.N., Seville, J.P.K., Parker, D.J., 2001b. Solids motion in rotating drums: bed turnover time and slumping – rolling transition. Powder Technol. (in press).

Das Gupta, S., Khakhar, D.V., Bhatia, S.K., 1991. Axial segregation of particles in a horizontal rotating cylinder. Chem. Eng. Sci. 46, 1513–1517.
Dolgunin, V.N., Ukolov, A.A., 1995. Segregation modelling of particles rapid gravity flow. Powder Technol. 83, 95–103.
Donald, M.B., Roseman, B., 1962. Mixing and de-mixing of solid particles: I – mechanisms in a horizontal drum mixer. Brit. Chem. Eng. 7, 749–753.
Elperin, T., Vikhansky, A., 1998. Granular flow in a rotating cylindrical drum. Europhys. Lett. 42, 619–623.
Fan, L.T., Shin, S.H., 1979. Stochastic diffusion model of non-ideal mixing in a horizontal drum mixer. Chem. Eng. Sci. 34, 811–820.
Gibilaro, L.G., Rowe, P.N., 1974. A model for segregating gas fluidised bed. Chem. Eng. Sci. 29, 1403–1412.
Haff, P.K., 1983. Grain flow as a fluid-mechanical phenomena. J. Fluid Mech. 134, 401–430.
Henein, H., Brimacombe, J.K., Watkinson, A.P., 1983. Experimental studies of transverse bed motion in rotary kilns. Met. Trans. B 14B, 191–205.
Henein, H., 1987. Radial segregation in rotary kilns: a review. In: Forrest-Holden, M.J. (Ed.), Rotary Kiln Technology. World Cement Publication, London, pp. 34–42.
Hill, K.M., Kakalios, J., 1995. Reversible axial segregation of rotating granular media. Phys. Rev. E. 52, 4393–4400.
Hirosue, H., 1980. Axial mixing of particles in rotating dryers and coolers. J. Chem. Eng. Jpn. 13, 365–371.
Hsiau, S.S., 2000. Effective thermal conductivities of a single species and a binary mixture of granular materials. Int. J. Multiphase Flow 26, 83–97.
Hsiau, S.S., Hunt, M.L., 1996. Granular thermal diffusion in flows of binary-sized mixtures. Acta Mech. 114, 121–137.
Hwang, C.L., Hogg, R., 1980. Diffusive mixing in flowing powders. Powder Technol. 26, 93–101.
Johnson, P.C., Jackson, R., 1987. Frictional–collisional constitutive relations for granular materials, with application to plane shearing. J. Fluid Mech. 176, 67–93.
Jenkins, J.T., Savage, S.B., 1983. A theory for the rapid flow of identical, smooth, nearly elastic, spherical particles. J. Fluid Mech. 130, 187–202.
Khakhar, D.V., McCarthy, J.J., Shinbrot, T., Ottino, J.M., 1997. Transverse flow and mixing of granular materials in a rotating cylinder. Phys. Fluids 9, 31–43.
Koga, J., Yamaguchi, K., Inoue, I., 1980. Mixing of solid particles of different density in a horizontal batch mixer, measurement of axial diffusion coefficient. Powder Technol. 26, 127–130.
Ktitarev, D., Wolf, D., 1999. A cellular automata for grains in a rotating drum. Comput. Phys. Commun. 121–122, 303–305.
Kudrna, V., Rochowiecki, A., 1988. Description of segregation in a horizontal drum mixer by use of the diffusion equation. Collect. Czech. Chem. Commun. 53, 771–787.
Kudrna, V., Hasal, P., Rochowiecki, A., 1992. Stochastic modelling of particle segregation in a horizontal drum mixer. Collect. Czech. Chem. Commun. 57, 2100–2112.
Levitan, B., 1998. Segregation and coarsening of granular mixture in a rotating tube. Physica A 249, 386–390.
Lun, C.K.K., Savage, S.B., Jeffrey, D.J., Chepurniy, N., 1984. Kinetic theories for granular flow: inelastic particles in Coutte flow and slightly inelastic particles in a general flow field. J. Fluid Mech. 140, 223–256.
Nakagawa, M., 1994. Axial segregation of granular flows in a horizontal rotating cylinder. Chem. Eng. Sci. 49, 2540–2544.
Nityanand, N., Manley, B., Henein, H., 1986. An analysis of radial segregation for different sized spherical solids in rotary cylinders. Met. Trans. B 17, 247–257.
Parker, D.J., Broadbent, C.J., Fowles, P., Hawkesworth, M.R., McNeil, P., 1993. Positron emission particle tracking—a technique for studying flow within engineering equipment. Nucl. Inst. Meth. Phy. Res. A326, 592–607.
Parker, D.J., Dijkstra, A.E., Martin, T.W., Seville, J.P.K., 1997. Positron emission particle tracking studies of spherical particle motion in rotating drums. Chem. Eng. Sci. 52, 2011–2022.
Pollard, B.L., Henein, H., 1989. Kinetics of radial segregation of different sized irregular particles in rotary cylinders. Can. Met. Quart. 28, 29–40.
Puri, S., Hayakawa, H., 1999. Dynamical behaviour of rotated granular mixtures. Physica A 270, 115–124.
Richman, M.W., Oyediran, A.A., 1992. Grain size reduction in granular flows of spheres: the effects of critical impact energy. J. Appl. Mech. 59, 17–22.

Rogers, A.R., Clements, J.A., 1971. The examination of segregation of granular materials in a tumbling mixer. Powder Technol. 5, 167–178.
Savage, S.B., 1998. Analyses of slow high-concentration flows of granular materials. J. Fluid Mech. 377, 1–26.
Savage, S.B., Hutter, K., 1989. The motion of a finite mass of granular materials down a rough incline. J. Fluid Mech. 199, 177–215.
Savage, S.B., Jeffrey, D.J., 1981. The stress tensor in a granular flow at high shear rates. J. Fluid Mech. 110, 255–272.
Savage, S.B., Lun, C.K.K., 1988. Particle size segregation in inclined chute flow of dry cohesionless granular solids. J. Fluid Mech. 189, 311–335.
Shen, H., Ackermann, N.L., 1982. Constitutive relationships for fluid–solid mixtures. In: Proceedings of the American Society of Civil EngineersJ. Eng. Mech. Division 108, 748–763.
Walton, O.R., Braun, R.L., 1993. Simulation of rotary-drum and repose tests for frictional spheres and rigid sphere clusters. In: Proceedings of Joint DOE/NSP Workshop on Flow of Particulates and Fluids, Ithaca, New York.
Wightman, C., Muzzio, F.J., 1998. Mixing of granular material in a drum mixer undergoing rotational and rocking motions – II: segregating particles. Powder Technol. 98, 125–134.
Williams, J.C., 1976. The segregation of particulate materials – a review. Powder Technol. 15, 245–251.
Yamane, K., 1997. Dynamics of granular flows, Ph.D. Thesis, University of Osaka, Japan.